The Effect of Structural Characteristics on the *In Vitro* Bioactivity of Hydroxyapatite

Donglu Shi, Gengwei Jiang, Jennifer Bauer

Department of Materials Science and Engineering, University of Cincinnati, Cincinnati, Ohio 45221

Received 6 June 2001; revised 20 August 2001; accepted 26 September 2001

Abstract: In previous studies a film of hydroxylapatite (HA) was coated onto the inner pore surfaces of reticulated alumina for bone substitutes with the use of a so-called thermal deposition method. In this process, the HA films must be sintered at high temperatures for a strong adhesion to the alumina substrate. It has been found that high-temperature sintering inevitably changes the crystallinity of the coated HA, and in turn affects its bioactivity. Therefore, in this study, *in vitro* experiments were carried out to investigate the effects of structural changes on the *in vitro* bioactivity. The factors dominating *in vitro* bioactivity of HA, including surface area, degree of crystallinity, and temperature, were identified. The activation energy for volume diffusion was calculated for different *in vitro* solution temperatures. Also discussed is the underlying mechanism of growth and dissolution processes during the *in vitro* test. © 2002 John Wiley & Sons, Inc. J Biomed Mater Res (Appl Biomater) 63: 71–78, 2002

INTRODUCTION

Among many bioactive ceramics and glasses, a particular bioactive ceramic in the calcium phosphate system,[1–6] hydroxyapatite (HA), $[Ca_{10}(PO_4)_6(OH)_2]$, exhibits good biological stability and affinity in *in vitro* tests at biological pH values.[7–13] It is believed that synthetic HA ceramic surfaces can be transformed to biological apatite through a set of reactions including dissolution, precipitation, and ion exchange. Following the introduction of HA to stimulated body fluid (SBF), a partial dissolution of the surface is initiated, causing the release of Ca^{2+}, HPO_4^{2-} and PO_4^{3-}, and increasing the supersaturation of the micro-environment with respect to the stable (HA) phase. A hydroxy-carbonate apatite (HCA) layer can form with the calcium and phosphate ions released from partially dissolving ceramic HA and from the biological fluids, which contain other electrolytes, such as CO_3^{2-} and Mg^{2+}. This polycrystalline HCA phase is equivalent in composition and structure to the mineral phase of bone. The *in vitro* reactivity of HA is governed by a number of factors, which can be considered from two aspects: *in vitro* environment and the properties of HA material. It is worth noting that most of the scientific publications deal with the former one. Intensive investigation had been done on the factors such as the type and concentration of the buffered or unbuffered solutions; pH of the solution; and degree of saturation of the solution. Fewer *in vitro* tests deal with HA material itself.

Extensive previous experiments have been focused on bioresorbability, interface growth, and surface-reaction kinetics of those bioactive materials in animals and humans.[15–22] Those studies have focused on (a) identifying the principal mechanisms that operate the interface bio- and chemical reactions between the implant material and soft/hard tissue, (b) studying the factors, such as composition, porosity size, and morphology, that dominate bioreactions, including bioresorbability, reaction kinetics, intergrowth rates, and (c) mechanical properties. Common characteristics of bioactive materials are the formation of a Ca-P–rich layer at the interface between the implant and bone.[1] It has been established that bioactivity occurs only within certain compositional limits.[23–28] Another factor that affects the bioactivity is the surface area, as it directly determines the dissolution rates of any solid materials. The porous structure of HA provides a template for fibrovascular ingrowth, which, when followed by osteoblast differentiation, results in the deposition of new lamellar bone. In the development of bone substitutes high porosity level is required for the following reasons:[29] (a) porous materials have large surface area, resulting in a high tendency to bioresorb, which induces bioactivity; (b) interconnected pores can provide a framework for bone growth into the matrix of the implant, and thus anchor the prosthesis with the surrounding bone, preventing loosening of implants, and (c) interconnected porosity acts like an organization of vascular canals, which can insure the blood and nutrition supply for the bone. To satisfy these requirements the dimension of the interconnected system must be at least 100 μm in diameter or a corresponding porosity of the order of 70%. Only when a large amount of pores are introduced into the

Correspondence to: Donglu Shi, Department of Materials Science and Engineering, University of Cincinnati, Cincinnati, Ohio 45221

DOI 10.1002/jbm.10087

TABLE I. Specimens Used in the *In Vitro* Test

Name	Source and Treatment	SSA (m^2/g)
HA	Commercial	63.02
HA600	HA heated at 600 °C, 30 min	40.92
HA900	HA heated at 900 °C, 30 min	17.45
SHA700	Synthesized HA heated at 700 °C, 4 h	15.19
SHA800	Synthesized HA heated at 800 °C, 4 h	1.49
SHA900	Synthesized HA heated at 900 °C, 4 h	1.23
1	HA heated at 700 °C, 3.5 h; particle size: 40 ~ 100 mesh	24.38
2	HA heated at 700 °C, 3.5 h; particle size: 100 ~ 200 mesh	25.70
3	HA heated at 700 °C, 3.5 h; particle size: <200 mesh	27.02

materials can reaction kinetics and intergrowth processes be enhanced.

As a result of its good tissue response, HA has been successfully used as bone filler, coating of orthopedic and dental implants, fillers of inorganic/polymer composites, substrate for the column chromatography of protein, and cellculture carrier. However, certain applications of porous bioactive ceramics have been restricted as a result of their low fracture strength and fatigue resistance. To overcome the weak mechanical properties of HA, coating of HA films has been attempted on the bioinert materials with high strength and toughness, such as alumina, zirconia ceramics, titanium metal, and titanium carbide. In evaluating HA coating methods, two factors are of primary importance. The first is whether the composition and properties of the coating are altered so that the *in vivo* performance of the coating is compromised. The second is that the coating should be strongly bonded to the substrate to maintain implant integrity as well to facilitate proper transmission of load from the implant to the surrounding bone. An HA coating that separates from the implant *in vivo* would provide no advantage over an uncoated implant and may be less desirable than no coating at all. In a worst-case condition, a weakly bonded HA coating may separate from the implant, and fragments of the coating would cause a variety of medical problems.

Mechanical properties and interfacial adhesion behavior are two important factors when one is considering the desirable properties of an implant coating. Therefore, in this study, particular attention was directed to the investigation of these two factors for the coated products. Fourier-transform infrared (FTIR) spectroscopy, X-ray diffractometry (XRD), scanning electron microscopy (SEM), thermal analysis methods, differential thermal analysis (DTA), and thermal gravimetric analysis (TGA) were used to examine the chemical and physical changes that occurred in the coating as a result of immersion in simulated body fluid (SBF) solution.

The objective of this research is centered on the effects of structural characteristics, particularly the effects of crystallinity and the surface area on the bioactivity and the reaction kinetics of both commercial and synthesized HA coating on a substrate of reticulated alumina. This work is a continuation of previous research, which accomplished a major step by establishing two HA coating techniques applicable for porous substrates. These two methods include a suspension method in which the ceramic substrates are first coated with a suspension containing the HA powder followed by sintering with a time–temperature cycle appropriate to the density of the HA coating. The other synthesis route, namely, thermal deposition (TD), involves mixing calcium Z-ethyl hexonate with bis(2-ethyhexl) phosphite stoichimetrically in ethanol. Detailed information about these two coating techniques on porous Al_2O_3 substrates has been published previously.[30–33] The study will also focus on the intent to obtain the fundamental knowledge about the temperature effect on bioactivity as a function of time and the activation energies for the different sintering temperatures of the HA specimens.

EXPERIMENTAL DETAILS

The *in vitro* tests were conducted to evaluate the bioactivity of the synthetic HA produced by synthesis methods. All the samples were tested in the powder form (Table I). For this work commercial HA and synthetic HA prepared by thermal deposition reported previously were tested. Table I summarizes the different heat treatments used to obtain a varied structural crystallinity in the materials. In HA700 three groups of samples with different specific surface areas (SSA) were tested.

The SBF solution that had ionic concentrations close to human blood plasma, as shown in Table II, was prepared by dissolving reagent-grade NaCl, $NaHCO_3$, KCl, $K_2HPO_4 \cdot 3H_2O$, $MgCl_2 \cdot 3H_2O$, $CaCl_2$, and Na_2SO_4 in ion-exchanged distilled water. The solution was buffered at pH 7.4 with 1M HCl and tris(hydroxymethyl) aminomethane ($(CH_2OH)_3CNH_2$) at 37 °C. Powders were immersed into solution at a 1-mg/ml ratio and maintained at 37 °C at periods ranging from 15 min to 9 weeks. The calcium concentrations in the solutions were measured by inductively coupled plasma (ICP). Subsequent

TABLE II. Ionic Concentrations of SBF in Comparison with Those of Human Blood Plasma

	Concentration (mM)							
	Na^+	K^+	Ca^{2+}	Mg^{2+}	HCO_3^-	Cl^-	HPO_4^{2-}	SO_4^-
Blood Plasma	142.0	5.0	2.5	1.5	27.0	103.0	1.0	0.5
SBF	142.0	5.0	2.5	1.5	4.2	147.8	1.0	0.5

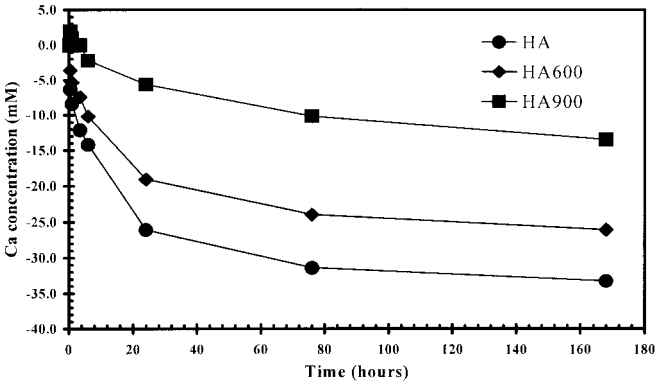

Figure 1. Ca concentration in SBF versus immersion time for the HA group sintered at temperature indicated.

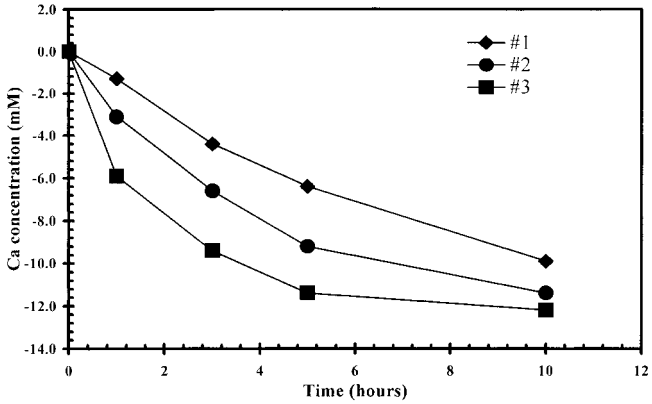

Figure 3. Ca concentration in the solution as a function of immersion time for Samples 1–3.

to immersion, the solutions were vacuum filtered. The powders were gently rinsed with alcohol and ion-exchanged distilled water, and then dried at room temperature. The surface microstructures before and after immersion of SBF solution were analyzed via scanning electron microscope (SEM). XRD and FTIR determined the contents of the phases that were present in the coatings. Measurements were obtained on a Philips X-ray diffractometer with CuK radiation at 35 kV and 23 mA.

RESULTS

Dissolution occurs from the bioactivity of the HA immersed in the SBF; this commonly releases Ca^{+2} among a few other elements. Figures 1 and 2 show the calcium concentration changes in the SBF solution as function of time. Both the HA and HA 600 led to an immediate uptake of the Ca concentration. Initially, there was a high rate of ion uptake, suggesting a new phase growing on HA surface in the supersaturated solution. After 24 h, with the depletion of supersaturation, the reaction proceeded at a lower rate of uptake. For HA900, there is an induction time of 60 min prior to a detectable decrease in Ca concentration, and the initial rate of Ca uptake is much lower than those of HA and HA600.

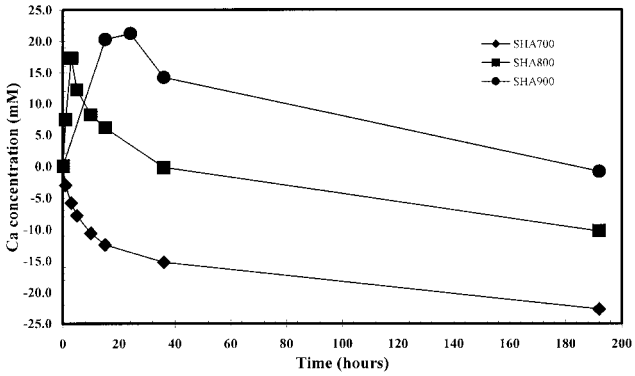

Figure 2. Ca concentration in SBF versus immersion time for the SHA group sintered at temperature indicated.

SHA700 behaved similarly to HA and HA600. However, like HA900, the reaction rate was slow. The reaction of SHA800 and SHA900 significantly differed from all above samples. During the first hour, an increase of Ca concentration was measured indicating that dissolution of SHA800 and SHA900 preceded the new phase formation. It was also noted that the rise in supersaturation for SHA900 was greater than that for SHA800. The ion uptake took place after this initial dissolution. Another difference between HA series and SHA series was that the latter took longer time to reach the solid/solution equilibrium stage, suggesting a slower reaction rate than that of HA series. These results indicate that the nucleation and growth of HA crystals onto the coating surface is critically dependent on the crystal structure developed in the HA coatings.

Figure 3 represents the Ca concentration in the solution as a function of immersion time for Samples 1–3. All these samples are commercial HA heat treated at 700 °C for 30 min. Therefore, these samples are of the same structural crystallinity but with different specific surface areas. They were tested at a ratio of 1 mg/ml SBF. It is apparent in Figure 3 that the rates of precipitation are highly dependent on the surface area. From these kinetic curves, the initial rate of precipitation, the slope of the first two data points, determined R_0. As shown in Figure 4, there is a linear relationship between the initial precipitation rate and the surface area.

Figure 5 is a plot of Ca concentration verses immersion time for HA, HA600, and SHA800, SHA900. Samples of each group have been selected to have the same surface area. As can be seen, the initial rates of HAs and SHAs separate into two branches. The HA group exhibits an initial gradual decrease, whereas that of SHA group increases quite rapidly. However, as can also be seen in this figure, calcium concentration of SHA 800 initially increases, but reaches a peak at 3 h, and thereafter decreases. In SHA900, although with a different rate, the calcium concentration always increases up to 9 h. SHA700 behaves similarly to HA and HA600 with a slow reaction rate, as can be seen in Figure 5. However, the

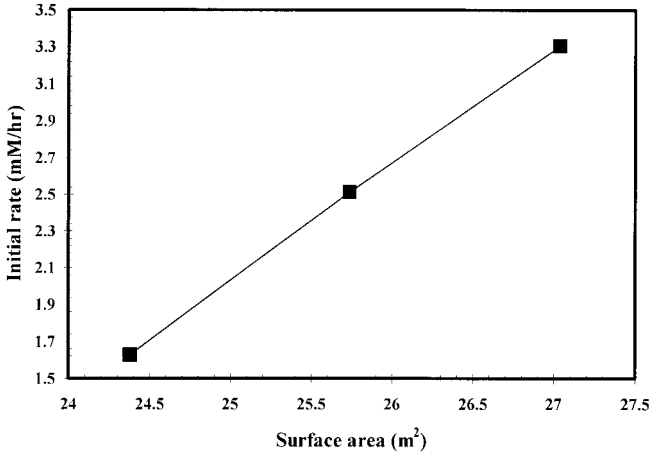

Figure 4. Initial reaction rate versus specific area for the samples shown in Figure 3.

reaction behaviors of SHA800 and SHA900 significantly differ from the HA samples. During the first hour, an increase of Ca concentration was measured, indicating that dissolution of SHA800 and SHA900 may have surpassed the new phase formation. It is noted that the rise in supersaturation for SHA900 is greater than that for SHA800. The ion uptake takes place after this initial dissolution.

Another difference between HA and SHA series is that the latter took longer to reach the solid/solution equilibrium stage, clearly indicating a slower reaction rate in the HA series. These results suggest that the dissolution and precipitation rates are critically dependent on the crystal structures developed in the HA samples.

DISCUSSION

Structural Effects

Based on the results, it is clearly seen that *in vitro* behavior of the HA coatings is strongly affected by the structural characteristics induced by heat treatment. The SBF used in this work represents human blood plasma, and it is supersaturated

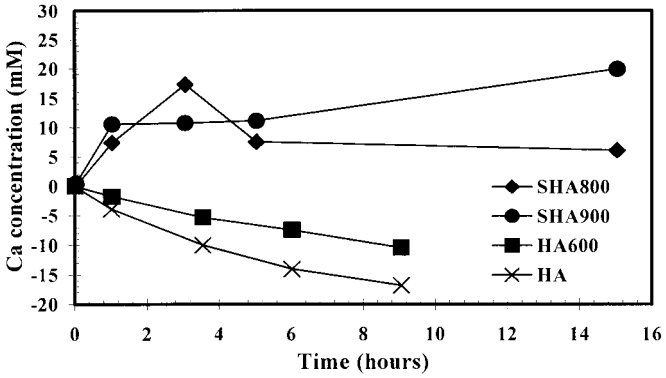

Figure 5. Ca concentration versus immersion time for some of the typical HA and SHA samples.

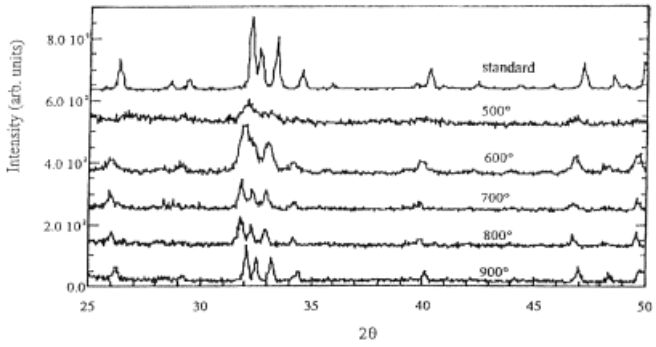

Figure 6. X-ray diffraction spectra for various HA samples heat treated at different temperatures.

with respect to HA. In this chemical environment, HA is the most stable phase among all the calcium phosphate phases; thus the HCA formation is thermodynamically possible. However, only HA, HA600, and SHA700 have led to immediate Ca ions uptake. HA900, SHA800, and SHA900 show a partial dissolution prior to precipitation. The difference in the dissolution ability of the HA samples is not the only factor in bioactivity.

Figure 6 shows XRD spectra of HA sintered at different temperatures in the range of 600–900 °C. The structural evolution begins from an amorphous state in the commercial HA. Crystalline phase started to form at 600 °C, and all peaks were attributed to the HA phase. In addition, relative peak intensities are in agreement with the expected values for HA. Therefore, it can be decided that the structure consists primarily of crystalline HA; no additional peaks were observed to appear at any firing temperatures. However, the peak shift could be noted by comparing with the standard XRD spectra of HA. At lower temperatures the shift was considerable, suggesting great lattice distortion. The breadth of the peaks was used as an indicator of crystal dimension in the direction perpendicular to the diffracting plane *hkl*. The crystal size *D* is inversely proportional to the peak breadth according to the Scherer equation:

$$D_{hkl} = \frac{K\lambda}{\Delta(2\theta)\cos\theta} \quad (1)$$

where D_{hkl} is the crystallite dimension; K is the Scherer constant (here $K = 0.9$); λ is the X-ray wavelength in Angstroms; $\Delta(2\theta)$ is the true broadening of the diffraction peak at half-maximum intensity. The contribution to the peak breadth from instrumental broadening was determined to be $\asymp 0.12°$ (0.002 radians), independent of 2θ. This amount, subtracted from the total experimental width, is the value of true broadening, assuming the two contributions add linearly. The peak breadth (D002) is given as a function of temperature in Figure 7. It can be seen that the peak breadth decreases with sintering temperature, indicating that the crystal size increases with increasing sintering temperature, from 600 to 900 °C. On the basis of the above analysis, it can be seen that the important

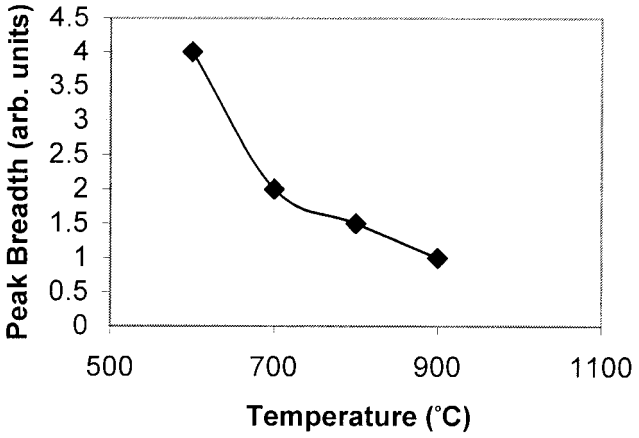

Figure 7. X-ray diffraction peak breadth versus temperature for the HA synthesized in this study.

difference with annealing temperature was the size of the individual crystals and the amount of crystal defects.

Based on XRD results shown in Figure 6 and 7 it can be seen that the heat-treated HAs have a varied degree of crystallinity.[33] The smaller crystals (low degree of crystallinity) would have higher surface energies compared to the large ones. Nucleation on these high-energy surfaces generally requires a smaller driving force or lower supersaturation than that for the induction of nucleation on a low-energy surface such as a well-crystallized surface. HA900, SHA800, and SHA900, therefore, must undergo an initial dissolution to reach the critical supersaturation at which it is possible for the new phase precipitation to occur.

It is possible that the crystal growth rate is controlled by more than one of the elementary rate-controlling mechanisms. The rate-controlling process can change depending upon particle size, solution concentration, and surface properties of the crystallites. The mechanisms of crystal growth are usually interpreted from measured reaction rates at different driving forces or from the activation energies of reactions. It is common practice to fit the data to an empirical rate law, which is represented by simple empirical kinetics:[34]

$$R_g = k_g s \sigma^n \tag{2}$$

where k_g is the rate constant for crystal growth, s is a function of the total number of available growth sites, and n is the effective order of reaction. A broad empirical test for growth mechanism can be achieved from a logarithmic plot of Eq. (2). From the n value, the probable mechanism can be deduced. It is possible that the crystal growth rate is controlled by more than one of the elementary rate-controlling mechanisms listed above. Under these circumstances, the rate-limiting steps may be dependent upon the jump frequency of lattice ions: (a) through the solution for mass transport control; (b) to the crystal surface for adsorption control, or (c) along the crystal surface or into a crystal lattice kink site for spiral and polynuclear control. The rate-controlling process can change depending upon particle size, solution concentration, and surface properties of the crystallites. A broad empirical test for growth mechanism can be achieved by plotting the data according to Eq. (2). An effective order reaction in the range $0<n<1.2$, $n\approx2$, or $n>2.5$ indicates that the rate-controlling process is one of adsorption and /or mass transport, surface spiral, or polynucleation, respectively. Experimentally, it is found that the growth rates of the calcium phosphates are insensitive to changes in fluid dynamics, indicating surface controlling mechanisms rather than mass transport of ions to the crystal surfaces.

Temperature Dependence of Activation Energy

Activation energies, obtained from experiments at different temperatures, may be used to differentiate between volume diffusion and surface-controlled processes. The activation energy for volume diffusion, reflecting the temperature dependence of the diffusion coefficient, usually lies between 16 and 20 kJ/mol, whereas for a surface reaction the value may be in excess of 35 kJ/mol. If a reaction has activation energy of less than 20 kJ/mol, it is safe to assume that it is overwhelmingly controlled by volume diffusion. However, if the activation energy is higher than 35 kJ/mol, it is quite certain that an adsorption process predominates. In all other cases, both adsorption and volume diffusion mechanisms may participate for a first-order reaction.

Figure 3 represents the Ca concentration in solutions as a function of immersion time at different surface areas. These samples were the same kind of powders to ensure that they had the same crystal structure and surface morphology; whereas the ratio of surface area to volume of SBF was different. It is apparent in Figure 3 that the rates of precipitation were highly dependent on the surface area. Based on the empirical kinetics [Eq. (2)], to build a relationship between the reaction rate R_g and surface area s, the degree of supersaturation σ should be kept at a constant value. The corresponding reaction rates were calculated by a simple fitting procedure from the above kinetic plots. As shown in Figure 4, there was a linear relationship between the precipitation rates and the total surface area, which is in agreement with the above empirical kinetics equation. This result also showed that crystallization occurred only on the added seed materials without any secondary nucleation or spontaneous precipitation. Furthermore, the advantage of porous bioceramics over dense bioceramics was proved by this relationship.

The initial precipitation rate was not used here because of the following considerations. First, the empirical fitting procedure used to calculate R_0 is greatly affected by the slower rates occurring after the initial fast stage of the precipitation process. Thus, the fitting data could not represent the true initial rate. Second, initial rate was a complicated factor. Rapid adjustment of surface composition usually happened when the solids were introduced into the growth or dissolution media. In the case of HA, initial uptaking surges were observed, which might be attributed to calcium ion adsorption. Therefore, considerable uncertainties can arise if too much emphasis is placed upon initial rates of reaction.

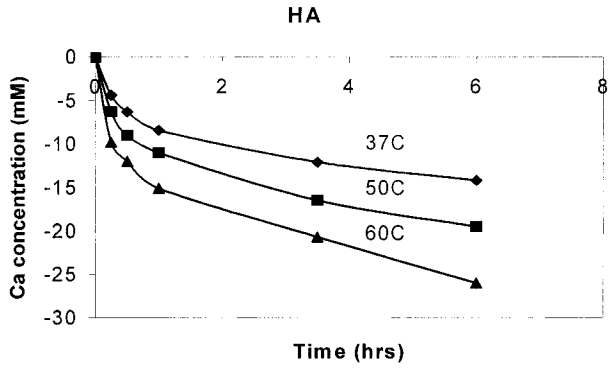

Figure 8. Ca concentration versus immersion time at the temperature indicated for HA.

Another important point is that, in this test, the different surface areas did not originate from the distribution of particle sizes, considering that different particle sizes might bring in the factor of surface morphology, which has great influence on the reaction rate. The effect of particle size would be demonstrated later. In the current method, the same powders were used, so that the factor of morphology was eliminated and a linear relationship was obtained.

The particles of different sizes behaved differently under the same SA/V test conditions. When the 40–100-mesh and <200-mesh particles at SA/V of 0.02 m^2/ml are compared, it is apparent that the Ca adsorption rate is slower for the smaller particles. This may be attributed to physical differences such as the radius of curvature and surface roughness.

Figure 5 is a plot of Ca concentration verses immersion time for HA, HA600 and SHA800, SHA900. Samples of each group were tested under the same SA/V ratio. As can be seen, the initial rate of HA was greater than that of HA600; the behavior of SHA800 differed from the one of SHA900. Therefore, it can be concluded that the specific surface area was not the only factor that affects the reaction behavior of various HA powders—the degree of crystallinity played an important role in their reaction rates.

Figures 8–11 show the calcium concentration as a function of time at different temperatures for samples of HA, HA600, HA900, and SHA700. It was apparent that the reaction rates were faster at higher temperatures.

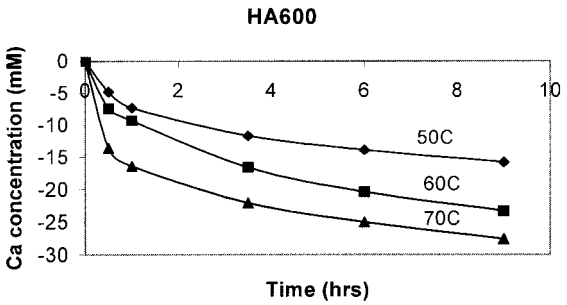

Figure 9. Ca concentration versus immersion time at the temperature indicated for HA600.

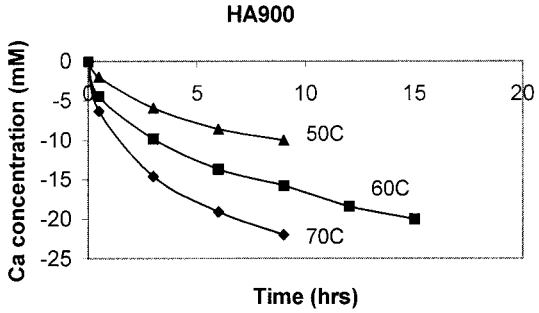

Figure 10. Ca concentration versus immersion time at the temperature indicated for HA900.

The chemical reaction in this case—the process of nucleation and crystal growth from solution—is described as an activated process with temperature, which is represented by the following relationship:

$$\text{rate} \propto \exp\left(-\frac{E_a}{kT}\right) \tag{3}$$

where E_a is the activation energy, so that reaction rate increases exponentially with temperature increase. The reaction-rate constant K is related to temperature by an Arrhenius equation:

$$K = K_o \exp\left(-\frac{E_a}{kT}\right) \tag{4}$$

By keeping σ at a constant value, plot $\ln R$ versus $1/T$, the slope of the curve will be E_a/k, and consequently E_a can be calculated.

According to the procedures described above, activation energy for HA, HA600, HA900, and SHA700 was computed. σ was selected at $\Delta\text{Ca} = -8$ mM for all the reaction temperatures. The computed activation energy was listed in Table III. The above results showed that the activation energy increased with the sintering temperature for HA powders. The activation energy of synthesized HA700 was much higher than those of HA and HA600.

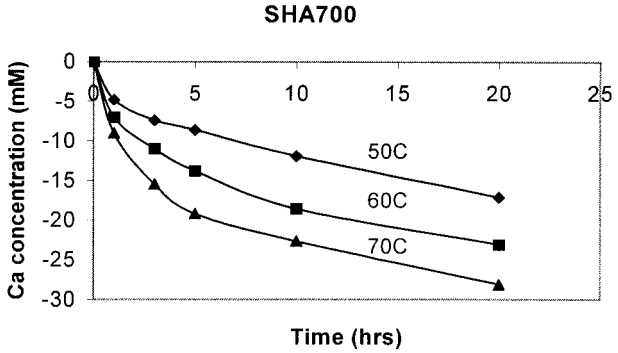

Figure 11. Ca concentration versus immersion time at the temperature indicated for SHA700.

TABLE III. Activation Energies for the Samples Indicated

Samples	Activation Energy (kJ/mol)
HA	66.3
HA600	80.3
HA900	172.7
SHA700	130.4

In vitro Biochemistry Behavior of HA

The formation of biological apatite on the surface of implanted synthetic calcium phosphate ceramics goes through a sequence of chemical reactions. It has been shown that the reaction rate *in vitro* appears to correlate with the rate of apatite mineral formation *in vivo*. Therefore the laboratory observations can be projected to the *in vivo* situation.

The *in vitro* behavior of bioceramics is determined by its stability at ambient and body temperatures. Many factors have significant influence on their stability, including the pH and supersaturation of the solution, crystallinity, structure defects, and porosity of the material.[35,36] Driessens[37] showed that, among the phases composed of calcium and phosphate, hydroxyapatite is the most stable at room temperature when in contact with simulated body fluid (SBF), which was used to represent the ionic concentrations of plasma. Generally, SBF will initiate a partial dissolution of the HA material, causing the release of Ca^{2+}, HPO_4^{2-}, and PO_4^{3-}, and an increasing in the supersaturation of the microenvironment with respect to HA phase that is stable in this environment. Following this initial dissolution is the reprecipitation. Carbonate ions, together with other electrolytes, which are from the biological fluids, become incorporated in the new apatite microcrystals forming on the surfaces of the ceramic HA.

Because any clinical use of calcium phosphate bioceramics involves contact with water, it is important to understand the stability of HA in the presence of water at ambient temperatures. As Driessens showed, there were only two calcium phosphate materials that were stable at room temperature when in contact with aqueous solution, and it was the pH of the solution that determined which one was the most stable. At a pH lower than 4.2, the component $CaHPO_4.2H_2O$ was the most stable, while at higher pH ($>$4.2), HA was the stable phase.

Therefore, in this *in vitro* test, at biological pH value, only HA can be found in contact with SBF. It is believed that synthetic HA ceramic surfaces can be transformed to biological apatite through a set of reactions including dissolution, precipitation, and ion exchange. Following the introduction of HA to SBF, a partial dissolution of the surface is initiated causing the release of Ca^{2+}, HPO_4^{2-} and PO_4^{3-}, and increasing the supersaturation of the microenvironment with respect to the stable (HA) phase. Carbonated apatite can form using the calcium and phosphate ions released from partially dissolving ceramic HA and from the biological fluids that contain other electrolytes, such as CO_3^{2-} and Mg^{2+}. These become incorporated in the new CO^{3-} apatite microcrystals forming on the surfaces of ceramic HA crystals. The *in vitro* reactivity of HA is governed by a number of factors, which can be considered from the two aspects: *in vitro* environment and properties of HA material.

CONCLUSION

In conclusion, structure characteristics, which are a combination of crystallinity and specific surface area, strongly affect the *in vitro* bioactivity of HA coatings. The bioactivity is reduced at higher degree of crystallinity, which is likely related to the high driving force for the formation of a new phase, and reaction rate is proportional to the surface area. The suggested underlying mechanism is that highly crystallized HA surface requires a high driving force for the formation of hydroxy-carbonate apatite (HCA) phase. The surface morphology and temperature also has a direct affect on the reaction rates of the HA coatings. The calcium absorption rate is slower for smaller particles; this could be attributed to physical differences including radius of curvature and surface roughness. The activation energy has increased with the heat treatment temperature for the HA powders.

REFERENCES

1. de Groot K. Biomaterials 1980;1:47.
2. de Groot K, Klein CPAT, Wolke JGC, de Blieck-Hogervorst JMA. In: Yamamuro T, Hench LL, Wilson J, editors. Handbook of bioactive ceramics. Boca Raton, FL: CRC Press; 1990. vol. 2, p 133–142.
3. de Groot K, Geesink R, Klein CPAT, Serekian P. J Biomed Mater Res 1987;21:1375–1381.
4. de Lange GL, de Putter C, Burger EH, de Groot K. In: Pizzoferrato A et al., editors. Proceedings of the Sixth European Conference on Biomaterials. Amsterdam: Elsevier; 1987. p 217–221.
5. Deer WA, Ahowie R, Zussman J. An introduction to the rock forming minerals. Hong Kong: Longman; 1985. p 504–509.
6. Aoki H. Medical applications of hydroxyapatite. Tokyo: Ishiyaku EuroAmerica; 1994.
7. Hing K, Best SM, Tanner KE, Revell PA, Bonfield W. Bioceramics 1996;9:157–160.
8. Best S, Sim B, Kayser M, Downes S. J Mater Sci Mater Med 1997;8:97–103.
9. Maxian SH, Zawadsky JP. J Biomed Mater Res 1993;27:717–728.
10. Bruder SP, Kraus KH, Goldberg VM, Kadiyala S. J Bone Joint Surg Am 1998;80:985.
11. Chistolini P, Ruspantini I, Bianco P, Corsi A, Cancedda R, Quarto R. J Mater Sci Mater Med 1999;10:739.
12. Klein C, de Groot K, Chen W, Li Y, Zhang X. Biomaterials 1994;15:31.
13. Rapamonti U, Ma S, Reddi AH. Matrix 1992;12:202.
14. Kokubo T. Biomaterials 1991;12:155–163.
15. Kokubo T, Ohtsuki C, Kotani S, Kitsugi T, Yamamuro T. In: Heimke G, editor. Bioceramics. German Ceramic Society; 1990. vol 2, p 113–120.
16. Kokubo T, Kushitani H, Ohtsuki C, Sakka S, Yamamuro T. J Mater Sci Mater Med, 1992;3:95–100.
17. Kokubo T. In: Hench LL, Wilson J, editors. An introduction to bioceramics. Singapore: World Scientific; 1993.

18. Kokubo T. J Non-Cryst Solids 1990;120;138–151.
19. Kokubo T, Shigematsu M, Nagashima Y, Tashiro M, Nakamura T, Yamamuro T, Higashi S. Bull Inst Chem Res Kyoto Univ 1982;60:260–268.
20. Kokubo T, Ito S, Shigematsu M, Sakka S, Yamamuro T. J Mater Sci 1987;22:4067–4070.
21. Andersson ÖH. Ph.D. dissertation, 'c2bo Akademi, Finland; 1990.
22. Fowle BO. Inorg Chem 1974;13:194.
23. Hench LL, Clark AE. Adhesion to bone, biocompatibility of orthopaedic implants. Boca Raton, FL: CRC Press; 1982. vol 2, p 129.
24. Hench LL. J Non-Cryst Solids 1975;19:27.
25. Hench LL. Stability of ceramics in the physiological environment. In Williams DF, editor. Fundamental aspects of biocompatibility. Boca Raton, FL: CRC Press; 1981. vol 1, p 67.
26. Hench LL. J Phys Paris 1982;43;C9.
27. Hench LL. Ann NY Acad Sci 1988:523;54.
28. Hench LL. J Non-Cryst Solids 1978;28.
29. Buckwalter JA, Cooper RR. Am Acad Orthop Surg 1987;36: 27.
30. Jiang G, Shi S. J Biomed Mater Res (Appl Biomater) 1998;43: 77.
31. Shi D, Jiang G. Mater Sci Eng C 1998;247.
32. Jiang G, Shi D. J Biomed Mater Res (Appl Biomater) 1999:48; 117.
33. Jiang G, Wen J, Shi D. J Biomed Mater Res (Appl Biomater) in press.
33. Nielsen AE. Ind cryst 1979:78;159.
35. Christofferssen J, Christoffersen MR. J Cryst Growth 1982;57: 21.
36. Margolis HC, Moreno EC. Calcif Tissue Int 1992;50:137.
37. Driessens FCM. In: de Groot K., editor. Bioceramics of calciumphosphate. Boca Raton, FL: CRC Press; 1983. p 1.